Appl. Phys. B 78, 93–102 (2004)
DOI: 10.1007/s00340-003-1331-3

Applied Physics B
Lasers and Optics

J. LUQUE[1,*]
P.A. BERG[1,**]
J.B. JEFFRIES[1,✉]
G.P. SMITH[1]
D.R. CROSLEY[1]
J.J. SCHERER[2]

Cavity ring-down absorption and laser-induced fluorescence for quantitative measurements of CH radicals in low-pressure flames

[1] Molecular Physics Laboratory, SRI International, Menlo Park, CA 94025, USA
[2] NovaWave Technologies, Redwood Shores, CA 94065, USA

Received: 2 June 2003
Published online: 18 November 2003 •

ABSTRACT The absolute, quantitative spatially resolved distribution of CH radicals was measured in the reaction zone of a low-pressure methane/air flame (25 Torr) using a combination of laser-induced fluorescence (LIF) and cavity ring-down (CRD) absorption spectroscopy operating on the $A\,^2\Delta$–$X\,^2\Pi(0,0)$ transition. The spatially resolved 1-D image of LIF provides a direct measure of the CH distribution along the path of the laser beam in the CRD cavity. The temperature distribution was determined from measurements on a pair of rotational transitions. A series of LIF line images and CRD absorption measurements taken at various burner heights are combined to form a quantitative 2-D image of the CH distribution. This is used to interpret the CRD measurements along this inhomogeneous path. The 10 ppm peak CH concentration measured here on the centerline of the flame is in good agreement (within 15%) with earlier CH A–X LIF measurements calibrated by Rayleigh and Raman scattering. A 1-D LIF image collected simultaneously with CRD absorption was also used to quantify and optimize the spatial resolution of the CRD measurement.

PACS 42.62.Fi; 82.33.Vx; 33.80.Gj

1 Introduction

Laser-induced fluorescence (LIF) imaging is a well-established method to determine the spatial distribution of reactive atoms and radical molecules. Such species are intermediate between feedstock and final products in chemically reactive systems such as flames and plasmas. As radicals are often present at low concentrations in flames, LIF provides the diagnostic of choice to obtain their spatial distribution [1–3]. Cavity ring-down (CRD) absorption spectroscopy has also demonstrated the ability to measure weak optical absorptions in flames, but only enables the determination of line-of-sight averaged concentrations. In this paper we combine these two methods to obtain the spatially resolved absolute concentration of the chemical intermediate CH radicals in the reaction zone of a low-pressure methane/air flame. To our knowledge, this work reports the first quantitative simultaneous CRD/LIF flame measurement [4, 5].

CRD has recently been used to detect CH using the C–X transition in atmospheric pressure [6, 7] and low-pressure [8] hydrocarbon flames. CRD on CH A–X has also been used to investigate CH in atmospheric pressure diamond-forming flames [9, 10]. In [11] CRD was used to obtain average CH concentrations in low-pressure (31 Torr) methane/oxygen/argon flames via the A–X band system. Previously, CRD was used to calibrate LIF measurements on the CH B–X systems, and distributions were obtained in a 25 Torr methane/oxygen/nitrogen flame and compared to detailed model calculations [12]. As advertised in that paper as well as in our similar CRD-LIF measurements on formaldehyde [13], here we report the details of both simultaneous and sequential schemes for CRD calibration of LIF distribution measurements. In this paper we use the CH A–X transitions and compare these measurements to our work [12] using B–X transitions and earlier results [14] using centerline LIF that was calibrated by Rayleigh and Raman scattering, and we find agreement to within 15%.

CRD and LIF provide complementary information and together form a very powerful diagnostic scheme. CRD provides a quantitative measurement of the line-of-sight absorption with extraordinary sensitivity [15]. However, like all absorption techniques, CRD only determines the line-of-sight integrated absorbance; thus, an independent determination (or in many cases an assumption) of the absorber distribution is required. Here we demonstrate that LIF can provide a direct measure of the absorber distribution in inhomogeneous flames, and that the combination of LIF and CRD provides a means to obtain a quantitative distribution of the target radical concentration. Additionally, we demonstrate that the combination of LIF and CRD can be utilized to understand as well as optimize the CRD spatial resolution.

2 Background

The CH radical has an important role in emission of NO_x in hydrocarbon flame exhaust [16, 17]. The published measurements of CH in flames comprise primarily detailed LIF studies [18], although other optical methods are represented [19]. CH is a precursor to NO in the reaction $CH + N_2$

✉ *Current address*: Mechanical Engineering Department, Thermosciences Division, Bldg. 520, Stanford University, Stanford, CA 94 305-3032, USA; Fax: +1-650/723-1748, E-mail: jay.jeffries@stanford.edu
*Lam Research Corporation, Fremont, CA 94 538, USA
**Coherent Inc., Santa Clara, CA 95 054, USA

in the prompt (Fenimore) mechanism [20] and destroys NO via the CH + NO reaction during NO_x reburn. This important chemical intermediate is present at mixing ratios of only a few parts per million (ppm); thus, determination of the absolute CH concentration requires quantitative measurements in harsh, reactive flame environments.

Prompt NO_x concentrations are predicted to be very sensitive to the absolute concentration of CH, so it is important to have accurate values of this quantity. Quantitative LIF measurements of trace radicals require that the fluorescence quantum yield as well as optical collection efficiencies are known (see Sect. 3.1). Quantitative LIF measurements were obtained first in 40 Torr propane/air flames [21], followed by near-stoichiometric 25 Torr methane/air flames [22]. Additionally, LIF data has been obtained as a function of fuel/air stoichiometry in low-pressure methane flames [14, 23]. The fluorescence quantum yield in these low-pressure flames was calculated from fluorescence lifetime measurements. Alternatively, the variation of fluorescence quantum yield in the flame can be suppressed by time gating the LIF promptly after excitation such that only a small fraction of the decay time is measured, although this scheme is limited to pressures ~ 50 Torr when ns lasers are used for time-resolved LIF measurements. Quantitative LIF has also been extended to CH measurements of atmospheric pressure flames [24] by calculating the fluorescence quantum yield from a model which combines the chemical composition and knowledge of the measured fluorescence quenching rates [25]. The optical collection efficiency can be determined from Rayleigh and/or Raman scattering calibration measurements. The CRD absorption method described below provides an alternative calibration scheme that is fully independent of these factors.

Absorption measurements have long been used to calibrate LIF measurements of OH in flames [26, 27]. These measurements, however, are relatively easy as the OH concentration in flames is roughly 1000 times larger than that of CH, and OH exists in both the flame-front and burnt-gas regions. Thus, single-pass direct absorption approaches have sufficient sensitivity to measure path-integrated OH concentration with good signal to noise. The OH distribution along the laser beam can be determined by imaging the LIF onto a linear-array detector, while simultaneous laser absorption may then be used to calibrate the OH distribution at some path above the burner. As the CH concentration in a hydrocarbon flame is significant only in the flame front, and is usually too low for direct absorption measurements, single-pass direct absorption strategies are not adequate. However, as demonstrated below, CRD provides the sensitivity needed to implement absorption-based CH calibration of LIF distributions.

3 Approach to absolute number densities

In this paper, we describe the use of a combination of LIF and CRD to determine two-dimensional (2-D) spatially resolved CH concentrations. Three sets of experiments are performed. First, LIF and CRD spectra are measured simultaneously, determining the CRD from the decay time of light exiting the cavity mirror at the exit to the burner chamber, while making a one-dimensional (1-D) image (onto a 2-D array) of the LIF produced by the weak intracavity CRD laser light. The LIF image is used to align the CRD cavity and optimize the spatial resolution of the CRD measurement. Second, CRD is used to make absolute CH absorbance measurements along the line of sight in the flame as a function of height above the burner surface. Third, the CRD mirrors are replaced by windows, and a series of 1-D LIF images of the CH in the flame were obtained as a function of height above the burner. A 2-D image is constructed from the measurements. The image shows the relative CH concentration along the line of sight after minor corrections concerning quenching and temperature distribution. We use this information together with the CRD times to derive absolute concentrations at any given point along the beam, for example at the centerline where the flame is closest to a one-dimensional flow.

In this section, we describe first the means of making absolute measurements by LIF and by CRD. Then we note the approach for simultaneous and sequential LIF-CRD. The overall experimental arrangement is shown in Fig. 1.

3.1 *Laser-induced fluorescence*

In absolute concentration determinations made solely by LIF, the transition is excited in a linear or nearly linear regime, and the subsequent fluorescence is collected and time resolved to determine the fluorescence quantum yield. The general equation describing the linear LIF signal from a level i in the ground state (S_i) assuming that the fluorescence is integrated over time and emission wavelength is

$$S_i = n\, f_B \frac{B}{c} E_L \frac{\Gamma(\nu)}{\Delta\nu} \frac{\tau_{eff}}{\tau_0} \frac{\Omega}{4\pi} \varepsilon\, \eta\, l. \quad (1)$$

Here, n is the number density, f_B is the Boltzmann fraction (number of molecules in the pumped ground-state level), B is the absorption coefficient, E_L is the laser energy, $\Gamma(\nu)/\Delta\nu$ is the direct absorption overlap integral $g(\nu)$ [28], $\Delta\nu$ is the laser bandwidth, τ_{eff} is the fluorescence lifetime, and τ_0 is the radiative lifetime. The term $\Omega\varepsilon\eta l$ includes the solid angle (Ω), the transmission efficiency of the optics (ε), the photoelectric efficiency of the light detector (η), and the effective optical path length (l). This product is determined by either Rayleigh or Raman scattering calibration [29, 30]. Details of this quantitative LIF approach, plus associated errors and examples, are given elsewhere [21, 22, 24, 31, 32]. Emission and absorption coefficients for temperature and number-

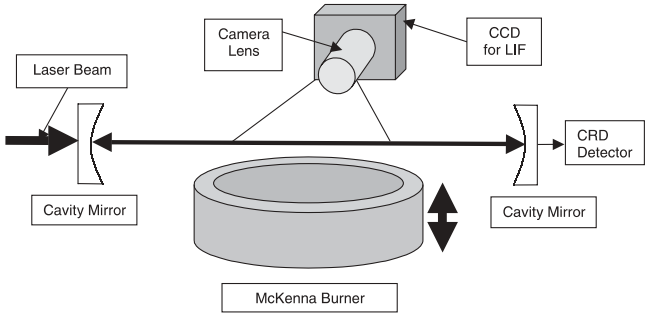

FIGURE 1 Schematic of the experiment for CRD and LIF simultaneous measurements in the low-pressure flame. Typical single-path LIF measurements are obtained by replacing the mirrors with quartz windows

density calculations are from the database LIFBASE [33] and published work [34]. This is the basis for previous determinations of absolute CH concentrations in this laboratory (using both the A–X and B–X band systems), which are here compared to the present results from CRD and relative LIF profiles across the flame. Other factors in this equation (f_B, B, and $\Gamma(\nu)/\Delta\nu$) are also required to convert CRD absorption cross sections $\sigma(\nu)$ to absolute number densities.

3.2 *Cavity ring-down absorption*

In a cavity ring-down experiment, the monochromatic light pulse coupled into the cavity decreases in intensity with time due to mirror, scattering, and absorption losses. The light intensity collected beyond the exit mirror on every other pass decays exponentially with a ring-down lifetime τ given by

$$\tau(\nu) = \frac{L}{c}\frac{1}{T + A + \sigma(\nu)nd}. \tag{2}$$

Here L is the cavity length, $T + A$ are mirror and scattering losses, $\sigma(\nu)$ is the cross section for the absorber, n is the number density of the absorber, and d is the distance in the path assuming the absorber is distributed homogeneously. Because the CH is not distributed homogeneously along the laser beam for the combined LIF/CRD measurement reported here, we will use the density-weighted path, furnished by LIF. Laser-intensity variations do not contribute to the uncertainty, as they would in typical absorption measurements, because the absorption is determined as a time decay. The difference between on-resonance and off-resonance absorption gives the sample absorbance:

$$\left(\frac{1}{\tau(\nu)} - \frac{1}{\tau_{\text{off}}}\right)\frac{L}{c} = \sigma(\nu)nd \tag{3}$$

and the absorption cross section is

$$\sigma(\nu) = B f_B h\nu g(\nu). \tag{4}$$

Here, $g(\nu) = \Gamma(\nu)/\Delta\nu$ is the line-shape integral.

The integrated absorbance over a spectral feature, sometimes called the equivalent width, is

$$\int \sigma(\lambda)\mathrm{d}\lambda = 10^{-7}\lambda_0 B h n f_B d. \tag{5}$$

It is calculated by integrating the absorbance in wavelength; λ_0 is the center spectral line wavelength (in nm). An advantage of analyzing integrated absorbance instead of single-wavelength absorption is that number-density measurements are less sensitive to finite laser bandwidth effects on CRD measurements as shown by Zalicki and Zare [35] and Yalin and Zare [36].

3.3 *Combined* LIF *and* CRD

Two types of experiments are performed which combine LIF and CRD measurements. To optimize the CRD spatial resolution, we image LIF along the weak laser beam in the cavity and simultaneously measure absorbance by CRD. The LIF image provides the spatial profile of the light inside the cavity and this image is used to optimize the cavity alignment [11, 37]. As discussed below, the spatial resolution of CRD is only optimal for light coupled into the TEM_{00} cavity mode, and the ring-down time alone is inadequate to insure TEM_{00} coupling. The simultaneous LIF measurement provides the independent measurement needed to optimize the spatial resolution. Good spatial resolution is particularly important when measuring reactive localized transients such as CH.

For a quantitative measurement of the inhomogeneous distribution of CH concentration, we calibrate the LIF with the CRD absorption measurement of column density. For these measurements, the LIF is acquired sequentially after CRD measurements as a function of height above the burner. After the CRD is measured, we remove the mirrors to enable a single pass of a more intense light pulse for LIF excitation that is coupled into the CRD cavity. A single pass enables a short time gate to significantly reduce the flame emission collected. We term this arrangement sequential LIF-CRD to distinguish it from the simultaneous measurements. LIF and CRD measurements are performed at each point above the burner. In Sect. 5, we will compare the CRD-calibrated LIF on the centerline of the flame to our previous Rayleigh-scattering calibrated LIF measurements.

4 Experiment

The flame studied is a laminar premixed 25.2 Torr CH_4/O_2 (30%)/N_2 (70%) flame of stoichiometric ratio 1.07 and flow rate 3.22 slm supported on a 6-cm-diameter sintered brass McKenna burner with a concentric argon shroud coflow of 0.5 slm. The CRD cavity axis is arranged for absorption measurements across the flat flame, and LIF signals are collected normal to the cavity axis; see Fig. 1. The burner is mounted on a motorized stage for vertical scans; the accuracy in the vertical scale is estimated to be 0.25 mm. The low-pressure flat-flame arrangement provides a test bed for combustion-chemistry mechanisms and the height above the burner on the centerline can be related to reaction time. The same flame has been extensively studied in our laboratory; we will compare the measurements reported here with previous measurements of centerline single-point LIF determination of gas temperature [14], calibrated LIF measurements of radical concentrations [14], and CRD-calibrated LIF [12, 13] of CH using the B–X transition. This flame has a nearly flat flame front $\sim$ 0.4-cm thick, which stands above the burner by $\sim$ 0.5 cm.

The CH $A\,^2\Delta$–$X\,^2\Pi$(0,0) band is excited near 430 nm by a pulsed dye laser (Lambda Physik LPD 3000, temporal width $\sim$ 6–7 ns, vertically polarized), pumped by a 355-nm Nd : YAG laser (Spectra Physics GCR-4). The laser spectral bandwidth measured with a monitor etalon is $0.13 \pm 0.01\,\mathrm{cm}^{-1}$. For selected CRD experiments, an intracavity etalon is used to improve the dye-laser bandwidth to $0.07\,\mathrm{cm}^{-1}$, slightly larger than the laser manufacturer specification of $0.05\,\mathrm{cm}^{-1}$ for this configuration. The shape of the laser bandwidth is described by a Gaussian for both arrangements. The spectral line shape characterization measurements were performed with an analyzing etalon before coupling the light into the cavity, and cav-

ity effects on the laser line shape, if any, were not evaluated. Laser-pulse energies between 1 μJ and 1 mJ were measured with a microjoulemeter (Rj-7200, Laser Precision Corp.).

After the CRD spatial resolution is optimized by simultaneous LIF-CRD (see below), CRD measurements are made as a function of height above the burner surface with a value every 0.35 mm to a height of 16 mm with the laser wavelength tuned on- and off-resonance of the CH transition. The flame is extinguished, the mirrors are replaced with windows, the height scale is calibrated, the flame is reproduced, and a set of on- and off-resonance line image LIF measurements are made at the same burner heights. LIF and CRD measurements are also made on two other rotational transitions on the same height scale to determine a two-line temperature field (LIF) and corresponding temperature height profiles (LIF and CRD).

4.1 *Cavity ring-down experiments*

The CRD mirrors, set in kinematic mounts, are used as the windows on the burner chamber and are spaced by 0.92 cm; 4-cm-diameter mounting arms isolate the mirrors from the flame gases in the 30-cm-diameter burner chamber (see Fig. 1). The mirrors have reflectivity better than 99.99% and a 6-m radius of curvature. The cavity confocal g is 0.85 with a theoretical TEM_{00} mode diameter of 950 μm (full width at $1/e^2$ intensity) [38] or a 600 μm full width at half maximum (FWHM). The estimated FWHM from simultaneous LIF during CRD, described below, is < 800 μm. Such a resolution is adequate for measurements in low-pressure flat flames where spatial distributions of chemical intermediates are several millimeters wide.

Spuler and Linne [39] have shown that the spatial resolution in a cavity with a confocal parameter of 0.85 is moderately insensitive to wave-front-curvature matching, but it is sensitive to mode matching. Thus, the coupled light must be mode matched to achieve this spatial resolution perpendicular to the cavity axis. The laser beam is spatially filtered with a telescope (2 : 1) and pinhole (100-μm diameter) for better mode matching to the CRD cavity. The cavity is initially adjusted for the longest CRD decay with the laser off-resonance with the CH absorption; however, the combined LIF and CRD measurements described below illustrate the care required to couple light into the cavity for optimal spatial resolution.

The laser energy hitting the front mirror before injection into the cavity is less than 10 μJ and the laser energy inside is less than 10 nJ, thus ensuring that the absorption is in the linear regime for strong transitions like CH A–X(0,0). We use CCD images of the ring-down laser light scattering in the chamber (at atmospheric pressure) to calibrate the distance above the burner. The spatial uncertainty is approximately ±0.25 mm, as judged by the reproducibility of profiles and our ability to determine the zero of the scale.

The signal light at the exit mirror is collected with a 9558QB EMI photomultiplier and digitized with a 500-MHz Tektronix 520C oscilloscope; a LabView program handles data acquisition and laser synchronization. The transients, averaged over 10–20 laser shots, are fitted to a single-exponential decay between 90% and 10% of the signal intensity. Absorbance profiles are measured by scanning the burner vertically with the laser on-resonance at the peak of a rotational line. It is well known that the off-resonance CRD background varies in the flame front. Some of the reasons for the variation are weak absorption of radicals, scattering of particles, and thermal gradient effects. Off-resonance profiles are recorded and subtracted to determine the absorbance profiles. The background variations are always less than 20 ppm per pass in absorbance units.

4.2 LIF *measurements*

LIF is used to obtain a series of one-dimensional horizontal overlapping images which are then assembled into a two-dimensional picture of the CH distribution throughout this nominally one-dimensional flat flame. The CH images are acquired with a gate of 20 ns. This gate is much shorter than the fluorescence effective lifetime of ∼ 90 ns for CH $A\ v' = 0$ in this flame [40], making corrections from quenching variations with composition and temperature negligible [41]. The rotational level is chosen to minimize the variations in fractional population (f_B) and line shape overlap integral in the temperature range where the CH radical is present in this flame – 1000 to 1800 K. The most favorable rotational levels in CH X, $v'' = 0$ are $N'' = 8$–10. To increase the signal-to-noise ratio the laser excitation is not strictly in the linear unsaturated regime. This is not a problem because the times for collisional deactivation and collisional relaxation in ground and excited states are longer than the laser excitation pulse in this low-pressure flame. After all these considerations the LIF image in Fig. 2 corresponds to the CH ground-state distribution in the flame. The 2-D CH distribution illustrates the deviation from a simple 1-D flat-flame geometry. At the edge of the burner, curvature of the flame front and diffusion effects are noticeable, and the flame curvature varies with argon shroud flow rates. For the flames examined here, which have feedstock flows to insure flame-standoff heights large enough to resolve the flame-front structure near the burner, this curvature is not negligible for line-of-sight measurements. Absolute number density normalization can be accomplished by methods previously reported in this flame by our group [14], which use Rayleigh-calibrated linear LIF, or by the peak number density extracted from combined CRD/LIF measurements reported here.

The ratio of the concentration spatial distributions from LIF measurements exciting two different rotational levels is used to obtain a temperature field. The lines utilized are Q_{2e} [6] and Q_{1f} [12], which have nearly identical absorption coefficients [34] and have negligible quenching variation with rotational level [41]. The temperature field obtained is shown in Fig. 2 (upper panel). High signal-to-noise ratios for these rotational level dependent CH spatial density distributions provide temperatures even in regions where the CH concentration is 10 times lower than the peak concentration. At the center of the burner we can measure temperatures between 2 mm and 8 mm above the burner surface, which vary from 1000 to 1800 K in that interval. Below 2 mm the temperature profile extrapolates smoothly to ∼ 300 K at the burner surface. Above 8 mm, the flame temperature has been extrapolated to 1900 K measured by OH A–X(0,0) LIF in a previous experiment in the same flame [14]. In spite of the limited flame-front

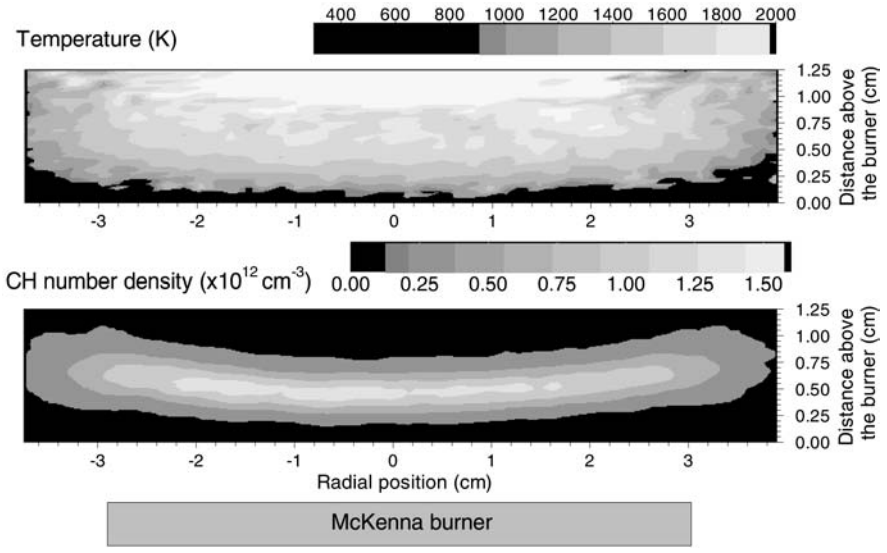

FIGURE 2 *Upper*: temperature field in the $CH_4/O_2/N_2$ flame at 25 Torr measured by two-line LIF using the CH A–$X(0,0)$ $Q_2(6)$ and the $Q_1(12)$ rotational lines. *Lower*: CH concentration spatial distribution in the same flame measured by excitation of the $Q_1(8)$ rotational line

distribution and low number density of the CH radical, it is feasible to use CH LIF to obtain a temperature profile in the region of the flame where the temperature gradient is important.

4.3 *Simultaneous* LIF *and* CRD

Although the amount of laser light coupled into a CRD cavity is only a small fraction of the initial laser pulse, this light circulates in the cavity for many round trips. Thus, CH is excited by a much less intense pulse that effectively has a much longer pulse length. For cavity mirrors of equal reflectivity and negligible losses by light scattering from the gas in the cavity, the target species is illuminated with half the laser fluence of the initial pulse. This LIF signal persists as long as there is light coupled into the cavity and, thus, the signal lifetime is significantly increased. Fluorescence is observable at these conditions because of the relatively high absorption coefficient of the CH A–X Q lines, high fluorescence quantum yields at 25 Torr, and multiple laser-pulse passes. LIF saturation should not be a factor because the rotational relaxation time of 20 ns and the fluorescence lifetime of 90 ns are much shorter than the typical ring-down time of 2 μs. The simultaneous LIF measurements require a time gate roughly similar to the ring-down times, which range between 2 and 20 μs in the present experiment, and therefore the simultaneous LIF measurements have much larger background luminosity than the normal single-path LIF measurements. In this experiment, the spatially resolved CH LIF from inside the CRD cavity directly indicates the spatial resolution of the CRD light circulating in the cavity, and we use the LIF image to optimize the spatial resolution in real time (30-s acquisition time) during the cavity alignment.

5 Results and discussion

5.1 *Cavity alignment*

To produce the best possible transverse spatial resolution, the light must only be coupled into TEM_{00}. To accomplish mode matching into TEM_{00}, it is important to carefully control the position of the beam relative to the optical axis of the cavity, the angle of incidence of the beam on the cavity, the spot size of the beam, and the radius of curvature of the wavefront. Figure 3 shows two CH LIF images taken simultaneously with CRD at a burner height near the peak of the CH distribution; an image of flame luminosity with the laser wavelength tuned off-resonance has been subtracted from both of these images. The top image illustrates the poor spatial resolution when light is coupled into higher-order modes; the spatial width of the LIF structure normal to the cavity axis has a FWHM of 0.22 cm. The bottom image shows the LIF from an optimized cavity alignment with a FWHM of 0.08 cm, which approaches the theoretical TEM_{00} beam waist for this cavity. Although the higher modes theoretically have a longer ring-down time, the difference is not large enough to use the ring-down time to select the proper cavity alignment for TEM_{00}. Thus, every cavity alignment is optimized by adjusting the mirrors for the longest off-resonance CRD decay time, then moving the laser wavelength resonant onto the $Q_1(8)$ CH A–$X(0,0)$ and ensuring that the beam waist approaches 0.08 cm as measured from the simultaneous laser-induced fluorescence. Figure 3 graphically illustrates the importance of direct measurement of cavity alignment and mode matching.

Cavity alignment by LIF monitoring is limited to species with fluorescent transitions and the alignment is biased towards the early portion of the ring-down transient. Ring-down times with CH A–$X(0,0)$ Q branch absorption are a few microseconds, and the LIF alignment method is less sensitive to the late part of the CRD transient. Other more general approaches have been reported in the literature. A quite general method was reported by Thoman and McIlroy [11] and later by Staicu et al. [37] and monitors the ring down with a CCD camera behind the exit mirror. Light coupled into modes other than TEM_{00} is observed as off-axis spots on the exit image, and the method can be time gated to observe the evolution of the light during the ring down, or time integrated to understand the total spatial resolution. Alternatively, Lee et al. [42] suggested a cavity alignment method which analyzes the cavity mode-beating behavior in the ring-down transient. Naus et al. [43] have aligned a stable resonator based on statistical noise properties of the decay transients. Recently, Evert-

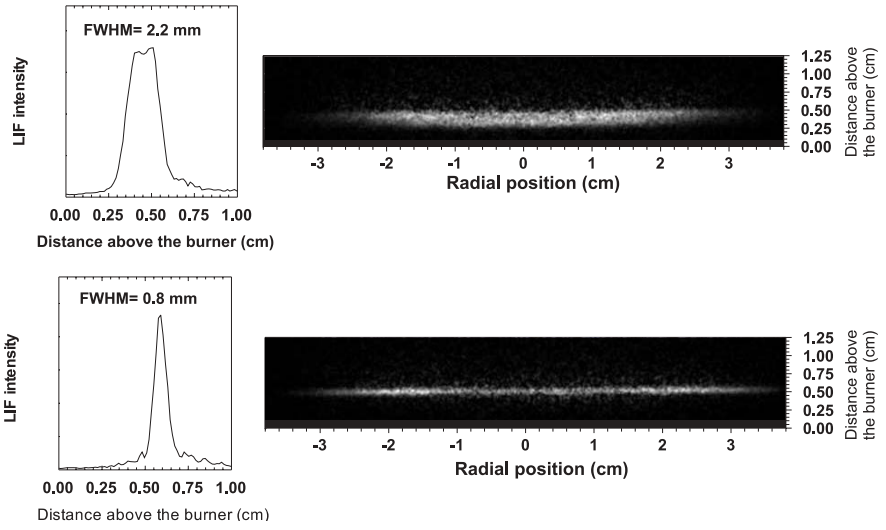

FIGURE 3 Laser-induced fluorescence recorded during cavity ring-down absorption of the CH A–X $Q_1(8)$ transition in a $CH_4/O_2/N_2$ flame at 25 Torr. *Lower*: optimized alignment for ring down. *Upper*: detuned laser-pulse circulation in the optical cavity. Both cases show the horizontally integrated signal on the *left*. The optimized alignment profile width corresponds to nearly TEM_{00} mode width. The non-optimized alignment shows a wide distribution with a double maximum indicating higher transverse modes in the cavity

sen [10] used Rayleigh and Mie scattering to align the cavity, just as we use LIF from the CRD beam. We also found that Rayleigh scattering was useful in our experiment for initial alignment when the burner chamber was filled with air at atmospheric pressure; however, a re-adjustment of the cavity was required when the chamber was evacuated, and the Rayleigh signal was too small to use at low pressure with or without the flame.

5.2 CRD *measurements*

Figure 4 shows a CRD absorption spectrum of the A–$X(0,0)$ Q branch near the CH distribution maximum in the flame front, and we can learn a lot from the relative absorption strengths on the various transitions. The off-resonance losses are roughly 250 ppm/pass and the largest CH (A–X) absorption on overlapped rotational transitions exceeds 1500 ppm/pass. This excellent signal to noise in Fig. 4 compares well with that observed by Thoman and McIlroy [11] in a similar optical cavity configuration. In Table 1, we select four satellite lines from Fig. 4 that are isolated and strong enough for a weak line measurement and ratio this absorbance with the associated main branch lines. The ratio of

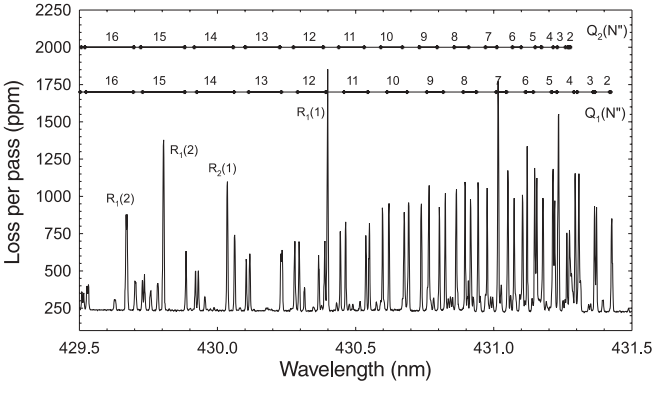

FIGURE 4 Cavity ring-down absorption spectrum of the CH A–$X(0,0)$ Q branch at 0.54 cm above the burner surface in a $CH_4/O_2/N_2$ flame at 25 Torr. The rotational temperature analysis of this spectrum provides a temperature of 1690 K

	LIF	CRD	Theory	CRD/ theory	LIF/ theory
$Q_{21}(2)/Q_1(2)$	0.13 ± 0.02	0.14	0.1	1.41	1.3
$Q_{21}(3)/Q_1(3)$	0.08 ± 0.02	0.085	0.065	1.31	1.23
$R_{21}(1)/R_1(1)$	0.29 ± 0.03	0.33	0.25	1.32	1.16
$R_{21}(2)/R_1(2)$	0.15 ± 0.02	0.18	0.14	1.29	1.07
Average				1.33	1.19

TABLE 1 Ratios of absorbance or LIF signals measured for R and Q main and satellite branches

CRD absorbance measurements is compared to the ratio predicted by the theoretical absorption coefficients [34] for weak to strong lines (satellite to main branch). This data suggests there are quantitative errors. For example, the Q_{21}/Q_1 and R_{21}/R_1 CRD line ratios are always larger than LIF results (taken from a previous experiment [34]). The deviations compared to line-strength theory are $\sim 20\%$ for LIF and $\sim 35\%$ for CRD. The LIF over-prediction can be explained by moderate saturation of the strong lines, whereas saturation is not an explanation for the CRD discrepancies [44]. The line-ratio data in Table 1 suggest that the simple single-exponential CRD ring-down analysis may under-predict the CH concentration by as much as 30% at the peak of the CH distribution. These discrepancies are consistent with those observed by Thoman and McIlroy [11] in a similar experiment using a laser with a similar bandwidth.

The finite laser bandwidth and the large CH absorption can produce significant departure from a single-exponential decay, and thus our analysis may introduce error. Numerous studies [7, 35, 36, 45–47] have been published to explain the deviation from single-exponential decay, provide alternative models for data analysis, and estimate errors introduced when a single-exponential analysis is used. The complication arises from different absorption at the line center and the wings of the line shape.

Yalin and Zare [36], extending previous work by Zalicki and Zare [35], have analyzed in a parametric fashion most of the relevant factors to assess finite bandwidth effects in the CRD pulsed experiments. Their analysis and systematic simulations use dimensionless parameters to characterize the

CRD experimental conditions: (i) the ratio Δ of transition bandwidth ($\Delta\nu$) to laser spectral bandwidth ($\Delta\nu_L$); (ii) the ratio κ of peak absorbance to background ring-down losses; (iii) the time interval for single-exponential fitting; (iv) transition line-shape and laser line-shape functions; and (v) the choice of analyzing peak absorbance versus area-integrated absorbance.

Typical values at the maximum CH concentration in our experiment are bandwidth ratio $\Delta = 0.7$, Gaussian laser and Gaussian transition line shape, peak absorbance to background $\kappa = 3.6$, and a single-exponential fit from 90%–10% of the decay. The estimated effect obtained by interpolating in their analysis for the strongest transitions at the peak of the CH distribution is $\sim 25\%$, a value that agrees well with our observed errors in the rotational line-strength ratios in Table 1. If we decrease the laser bandwidth with the dye-laser intracavity etalon, the bandwidth ratio is $\Delta = 0.4$ and the peak absorbance to background ratio is $\kappa \sim 4.5$. For this condition, the predicted effect is only a $\sim 5\%$ reduction in the measured absorbance for the strongest line at the peak of the CH concentration.

Figure 5 compares CRD spectra recorded with an etalon ($0.07\,\mathrm{cm}^{-1}$) and no etalon ($0.13\,\mathrm{cm}^{-1}$) at the peak of the CH distribution ($h = 0.54$ cm). The spectral line bandwidths are determined to be $0.20 \pm 0.01\,\mathrm{cm}^{-1}$ and $0.22 \pm 0.02\,\mathrm{cm}^{-1}$ respectively, and consistent with a Gaussian convolution of the Doppler broadening at 1700 K and the laser line shape. The spectrum with etalon has peak absorbances higher by 25% compared to those without the etalon. A calculation of the direct absorption overlap integral gives an increase of $\sim 13\%$ in the overlap due to the etalon in the laser cavity. The additional increase of $\sim 15\%$ observed in the experiment is because the CRD transient is better described by a single exponential, and is consistent with Yalin and Zare's analysis [36]. Area integration eqn. (5) and peak absorbance eqn. (3) quantification of the CRD results with the narrow laser spectral bandwidth provide nearly identical number densities, as expected from linear CRD behavior. These results once again illustrate finite bandwidth effects in CRD analysis, as well as the advantages of working with narrower laser line widths and matching the absorption strength to the empty-cavity losses.

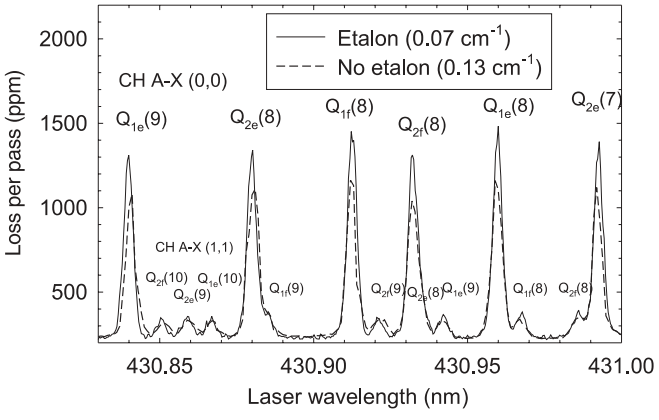

FIGURE 5 Section of the CH A–$X(0,0)$ Q-branch CRD spectrum at the peak of the CH spatial distribution obtained using two different dye-laser spectral bandwidths: *solid line* shows data with an etalon in the dye-laser cavity and *dashed line* shows data without the etalon

5.3 CRD *and* LIF *comparison*

5.3.1 Number densities. The CRD absorption measurements are line-of-sight integrated, and thus are measurements of column density. Because of the flame structure observed in Fig. 2, it is instructive to compare the CRD to a LIF column density determined by numerically integrating each line of sight in the LIF distribution in Fig. 2, and calibrating the LIF using our previous LIF Rayleigh determination [14]. The dashed line in the upper panel a of Fig. 6 plots the integrated LIF column density as a function of height above the burner, and the solid and open points are the CRD column density data

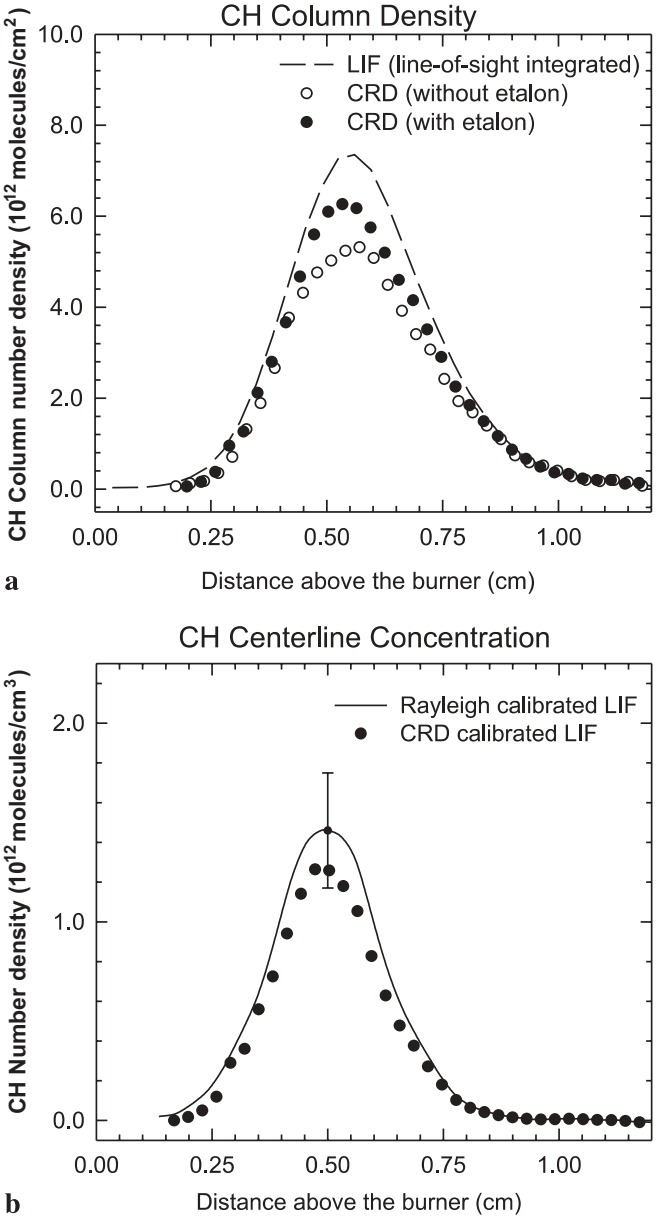

FIGURE 6 **a** Comparison of CH column-density profiles from CRD (*points*) with the equivalent path-integrated LIF (*dashed line*). CRD measurements with etalon (*solid circles*) and without etalon (*open circles*) in the dye-laser optical cavity illustrate the influence of the finite laser bandwidth on the CRD result. **b** *Solid line* shows CH concentration profile at the center of the flame from LIF normalized with Rayleigh-calibrated values [14, 22] and *points* show CRD-calibrated LIF

with and without the dye-laser etalon, respectively. The line-of-sight integrated LIF has a CH maximum column density of $(7.3 \pm 1.5 \times 10^{12}\,\mathrm{cm}^{-2})$, which compares very well with the CRD maximum column density of $(6.2 \pm 1.0 \times 10^{12}\,\mathrm{cm}^{-2})$, and the 15% difference is well within the combined uncertainties. Correction using the Yalin and Zare data [36] would raise the CRD column-density value by an additional 5% to $(6.5 \pm 1.0 \times 10^{12}\,\mathrm{cm}^{-2})$, and the difference between the two experiments using different calibration methods is only 11%. Note that the CRD measurements depend on the laser line width, and the peak CH values inferred from the CRD measurements without the etalon are an additional 20% lower as expected from our estimate of the fitting errors for large κ and Δ. Therefore, CRD calibration of LIF requires careful consideration of the finite bandwidth fitting errors of the CRD transients.

The calibration of LIF distributions with CRD can be compared to our previous absolute LIF point measurements on the centerline of the burner. If the CH distribution was uniform, the average concentration would simply be the (CRD column density) × (normalized LIF per unit length). For this experiment, the (LIF signal) ∼ (concentration × calibration constant), because the LIF quantum yield and the Boltzmann fraction for the $Q_1(8)$ excitation have negligible variation as we integrate across the flame. Therefore: $n_{\mathrm{CH}}\,(\mathrm{cm}^{-3}) = $ (CRD column density in molecules/cm^{-2}) × (normalized LIF signal in cm^{-1}).

However, the CH distribution is not uniform and, to compare with the previous work, we must consider the CH concentration on the centerline: (normalized LIF signal in cm^{-1}) = (centerline LIF signal in cm^{-3})/(line integral of the LIF signal in cm^{-2}).

In the lower panel b of Fig. 6, the points plot the centerline CH density calibrated by CRD at each height above the burner for the data from Fig. 2. Note that the flame curvature moves the peak of the CRD (or LIF) measurement of column density in Fig. 6a significantly further from the burner than the CH concentration on the centerline in Fig. 6b. The CRD-calibrated LIF centerline CH concentration compares well with our previous Rayleigh-calibrated LIF measurements [14] (the solid line in Fig. 6b). The Rayleigh calibration was performed only at the peak of the distribution, and this error bar is shown in Fig. 6b. The CRD-calibrated LIF concentration peak value on the centerline of $1.25 \times 10^{12}\,\mathrm{cm}^{-3}$ agrees well with the previous Rayleigh-calibrated LIF peak concentration value of $1.5 \times 10^{12}\,\mathrm{cm}^{-3}$. If we correct the CRD measurement with the 5% increase predicted by Yalin and Zare for our experimental conditions, the CRD-calibrated LIF rises to a peak value of $1.31 \times 10^{12}\,\mathrm{cm}^{-3}$, only 13% smaller than the Rayleigh-calibrated value.

The shape of the structure of the CH column density measured by CRD is in good agreement with the line-of-sight integrated LIF measurements. However, the curvature of the flame moves the peak in the CH column density 0.65 mm further from the burner surface than the peak of the centerline concentration. In addition, at burner heights above the flame front, the CH column density is significantly broadened compared to the centerline concentration. Therefore, the shape of the CH distribution would not have been captured had we simply assumed a uniform flat flame 6 cm in diameter. In addition, the peak concentration extracted from only a CRD measurement would have been 40% low.

These low-pressure burners have been an excellent test bed for detailed models of finite-rate chemistry, and the position of the maximum concentration of an intermediate radical species above the burner is a crucial test of the chemical mechanism. In addition, the shape of the radical species concentration profile is a good measure of the production and destruction loss rates. Thus, the use of CRD-only absorption measurements to test flame chemistry requires a very good understanding of the spatial distribution of the flame to insure fidelity of the comparison of the CRD column-density structure to the model-predicted concentration profile. Although absorbance data along radial chords would allow an Abel inversion correction to the CRD-only column density data [37, 48], LIF spatially resolved measurements have the advantage for non-cylindrical symmetry or unsteady structures where single-shot data potentially could be used. The value of the combined LIF distribution and CRD column-density measurements is illustrated by the data in Fig. 6b for one key species in chemical model validation.

The LIF values are slightly larger than CRD number densities [12, 13], indicating a small systematic error in either or both measurements. Kinetic modeling of the flame [14] with the GRI-Mech 3.0 mechanism [17], which is optimized with similar LIF data [22], predicts a peak CH number density of $1.5 \times 10^{12}\,\mathrm{cm}^{-3}$, whereas calibration of the LIF with the CRD data produces a centerline peak value of $1.35 \times 10^{12}\,\mathrm{cm}^{-3}$. Thoman and McIlroy [11] observed a similar trend in CH CRD results in CH_4/O_2 low-pressure flames compared to GRI-Mech 3.0 kinetic models. Mercier et al. [49] have also found their CH CRD concentrations to be ∼ 25% lower than the GRI-Mech 3.0 predictions. Whether this discrepancy is experimental or a model over-prediction is not clear.

5.3.2 Temperatures. Temperature measurement by line-of-sight absorption must be approached carefully, and the interpretation of the data can be very complicated if the absorber is not uniformly distributed along the line of sight with a uniform temperature. Temperature is determined via the Boltzmann distribution by the ratio of the populations in two different quantum states of the absorber. A sensitive temperature measurement requires a large energy difference between the two probed levels; however, if there is significant temperature non-uniformity along the path the selected probed levels can bias the measurement hot or cold. For the typical experimental condition of a cold boundary layer near the walls, this bias can be further exacerbated by the increase in density in colder regions. These issues have been studied for chemically stable combustion products which have significant populations in the cold boundary layers [50, 51], and will not be further discussed here.

These problems are not significant for CH in these stable, premixed flames for several reasons. First, CH is a combustion intermediate and only exists in the flame front in the limited temperature range 1000–2000 K. Second, we have chosen transitions, $Q_2(6)$ and $Q_1(12)$, which are nearly optimum for this temperature range. Since these two transitions have similar absorption strength, differing by less than a factor of two for temperatures larger than 1500 K, and less than a factor of

four for temperatures between 1000 and 1500 K, we expect similar finite bandwidth fitting errors will cancel in the ratio used to extract temperature.

Figure 7 shows vertical temperature profiles from LIF and CRD measurements. The solid line is the set of OH A–X measurement points on the centerline from a previous experiment in the same flame [14]. There are three LIF temperature distributions extracted from the CH LIF data in the upper panel of Fig. 2. The LIF temperature near the edge of the flame (solid squares) and that on the centerline (open triangles) shows the very limited temperature range where CH has significant concentration. Comparing the edge temperature profile to the flame center, there is a delay in the temperature rise. The edge profile is as much as 2 mm late and the maximum temperature is ~ 400 K less than at the center of the flame, a shape expected from the flame curvature.

The temperature profile calculated from integrating the LIF along the line of sight (open circles) provides a direct comparison to the CRD temperature (solid circles). The influence of flame curvature becomes noticeable for both line-of-sight data sets at heights above the peak in the CH distribution, illustrating the density weighting of edge regions for both measurements. There are two well-defined regions with respect to the CH distribution peak value at the flame center. Before the maximum, the high CH density is at the center of the flame. However, beyond the maximum the density is higher towards the edge of the flame. This distribution explains why the horizontally integrated LIF matches the center of flame temperature profile at distances below the CH maximum and declines toward the edge temperature profile above the CH density maximum. The CRD temperature profile agrees remarkably well with the line-of-sight integrated LIF temperature profile, which demonstrates that the CRD fitting errors do nearly cancel for the temperature measurements. For measurements of the important flame region below the flame front, the CRD temperature profile only deviates a maximum of 7% from the LIF temperature at the center of the flame at a height of 2 mm above the peak of the CH profile, and the CRD temperature profile does not show significant distortion either in shape or position.

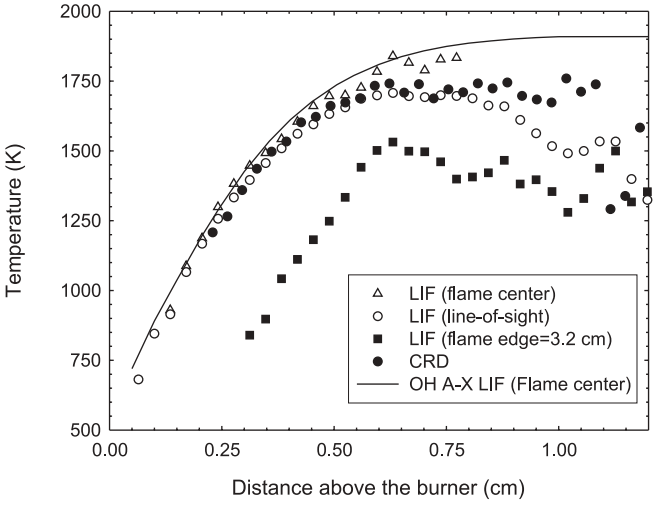

FIGURE 7 Temperature profiles in the $CH_4/O_2/N_2$ flame at 25 Torr. *Solid line*: OH A–X LIF measurements from Berg et al. [14] taken at the center of the burner. *Triangles*: CH A–X two-line LIF temperature profile at the center of the burner (integrated over 0.6 cm in the horizontal direction). *Solid squares*: CH A–X two-line LIF temperature at the edge of the burner (radial position 3.2 cm, integrated over 0.4 cm). *Open circles*: CH A–X two-line LIF temperature from line of sight (integrated over 8 cm in the horizontal direction). *Solid circles*: CH A–X two-line CRD absorption temperature

6 Conclusions

The combination of LIF and CRD measurements provides a powerful tool for quantitative measurements of gas-phase radical species. LIF provides the spatially resolved distribution and CRD the quantitative column density. The combination is significantly more quantitative than either method alone, and CRD calibration is much less laborious than Rayleigh-calibrated LIF. For a non-homogenously distributed absorber, concentration determination by CRD-only measurements requires independent knowledge of the path length and absorber distribution. Similarly, LIF-only measurements require calibration of the collection geometry and an absolute measure of the quantum yield. Thus, the two techniques are complementary, and CRD provides the sensitive method of absorption needed to calibrate spatially resolved LIF data. The CRD-calibrated LIF concentration measurements of CH in this low-pressure flame agree well with previous quantitative LIF calibrated by Rayleigh scattering and provide similar accuracy [12].

The spatial resolution of CRD in the direction normal to the cavity axis depends on mode coupling the light into the cavity, and only TEM_{00} has the optimum beam waist for spatially resolved measurements. If the absorber is not homogeneously distributed the variation of spatial resolution with cavity mode can complicate interpretation of the CRD measurement. Thus, the spatial mode of the optical coupling must be determined when the cavity is aligned. Simultaneous LIF/CRD is shown to provide a direct measurement of spatial resolution.

ACKNOWLEDGEMENTS This research was sponsored by the Basic Research Program of the Gas Research Institute and the NASA Earth–Sun Program.

REFERENCES

1 A.C. Eckbreth: *Laser Diagnostics for Combustion Temperature and Species* (Gordon and Breach, Amsterdam 1996)
2 K. Kohse-Höinghaus: Prog. Energy Combust. Sci. **20**, 203 (1994)
3 A.K. Hays, A.C. Eckbreth, G.A. Campbell (eds.): *Process Diagnostics: Materials, Combustion, Fusion, Materials Research* (Materials Research Society, Pittsburgh, PA 1988)
4 J.B. Jeffries: 'Applications of Laser-induced Fluorescence for Atmospheric and Combustion Diagnostics'. In: *Western States Section Meet. Combustion Institute, 2000*
5 A. McIlroy, J.B. Jeffries: *Cavity Ringdown Spectroscopy for Concentration Measurements, Applied Combustion Diagnostics*, ed. by K. Kohse-Höinghaus, J.B. Jeffries (Taylor & Francis, New York 2002) p. 98
6 X. Mercier, P. Jamette, J.F. Pauwels, P. Desgroux: Chem. Phys. Lett. **305**, 334 (1999)
7 X. Mercier, E. Therssen, J.F. Pauwels, P. Desgraoux: Combust. Flame **125**, 656 (2001)
8 I. Derzy, V.A. Lozovsky, S. Cheskis: Chem. Phys. Lett. **306**, 319 (1999)
9 R. Evertsen, R.L. Stolk, J.J. ter Meulen: Combust. Sci. Technol. **149**, 19 (1999)
10 R. Evertsen, J.A. Van Oijen, R.T.E. Hermanns, L.P.H. De Goey, J.J. ter Meulen: Combust. Flame **132**, 34 (2003)
11 J.W. Thoman Jr., A. McIlroy: J. Phys. Chem. A **104**, 4953 (2000)

12 J. Luque, J.B. Jeffries, G.P. Smith, D.R. Crosley, J.J. Scherer: Combust. Flame **126**, 1725 (2001)
13 J. Luque, J.B. Jeffries, G.P. Smith, D.R. Crosley: Appl. Phys. B **73**, 731 (2001)
14 P.A. Berg, D.A. Hill, A.R. Noble, G.P. Smith, J.B. Jeffries, D.R. Crosley: Combust. Flame **121**, 223 (2000)
15 G. Berden, R. Peeters, G. Meijer: Int. Rev. Phys. Chem. **19**, 565 (2000)
16 J.A. Miller, C.T. Bowman: Prog. Energy Combust. Sci. **15**, 287 (1989)
17 G.P. Smith, D.M. Golden, M. Frenklach, N.W. Moriarty, B. Eiteneer, M. Goldenberg, C.T. Bowman, R.K. Hanson, S. Song, W.C. Gardiner, V. Lissianski, Z. Qin: GRI-Mech 3.0
web site: http://www.me.berkeley.edu/gri_mech/ (1999)
18 K.C. Smith, D.R. Crosley: *Detection of Minor Species with Laser Techniques, Applied Combustion Diagnostics*, ed. by K. Höinghaus, J.B. Jeffries (Taylor & Francis, New York 2002) p. 9
19 K. Kohse-Höinghaus, J.B. Jeffries (eds.): *Applied Combustion Diagnostics*, in *Combustion* (Taylor & Francis, New York 2002)
20 C.P. Fenimore: Proc. Combust. Inst. **13**, 373 (1971)
21 J. Luque, D.R. Crosley: Appl. Phys. B **63**, 91 (1996)
22 J. Luque, G.P. Smith, D.R. Crosley: Proc. Combust. Inst. **26**, 959 (1996)
23 P.A. Berg, G.P. Smith, J.B. Jeffries, D.R. Crosley: Proc. Combust. Inst. **27**, 1377 (1998)
24 J. Luque, R.J.H. Klein-Douwel, G.P. Smith, J.B. Jeffries, D.R. Crosley: Appl. Phys. B **75**, 779 (2002)
25 J. Luque, R.J.H. Klein-Douwel, J.B. Jeffries, D.R. Crosley: Appl. Phys. B **71**, 85 (2000)
26 H.M. Hertz, M. Aldén: Appl. Phys. B **42**, 97 (1987)
27 K. Kohse-Höinghaus, J.B. Jeffries, R.A. Copeland, G.P. Smith, D.R. Crosley: Proc. Combust. Inst. **23**, 1857 (1988)
28 W.P. Partridge, N.M. Laurendeau: Appl. Opt. **34**, 2645 (1995)
29 J.T. Salmon, N.M. Laurendeau: Appl. Opt. **24**, 65 (1985)
30 W.K. Bischel, D.J. Bamford, L.E. Jusinski: Appl. Opt. **25**, 1215 (1986)
31 J. Luque, W. Juchmann, J.B. Jeffries: Appl. Opt. **36**, 3261 (1997)
32 J. Luque, W. Juchmann, J.B. Jeffries: J. Appl. Phys. **82**, 2072 (1997)
33 J. Luque, D.R. Crosley (eds.): LIFBASE: Database and spectral simulation for diatomic molecules, SRI International, MP-99-0099, www.sri.com/cem/lifbase (1999)
34 J. Luque, D.R. Crosley: J. Chem. Phys. **104**, 2146 (1996)
35 P. Zalicki, R.N. Zare: J. Chem. Phys. **102**, 2708 (1995)
36 A.P. Yalin, R.N. Zare: Laser Phys. **12**, 1065 (2002)
37 A. Staicu, R.L. Stolk, J.J. ter Meulen: J. Appl. Phys. **91**, 969 (2002)
38 M. Young: *Optics and Lasers: Including Fibers and Optical Waveguides* (Springer, Berlin 2000)
39 S. Spuler, M. Linne: Appl. Opt. **41**, 2858 (2002)
40 M. Tamura, P.A. Berg, J.E. Harrington, J. Luque, J.B. Jeffries, G.P. Smith, D.R. Crosley: Combust. Flame **114**, 502 (1998)
41 J. Luque, D.R. Crosley: Appl. Opt. **99**, 1423 (1999)
42 D.H. Lee, Y. Yoon, B. Kim, J.Y. Lee, Y.S. Yoo, J.W. Hahn: Appl. Phys. B **74**, 435 (2002)
43 H. Naus, I.H. v. Stokkum, W. Hogervorst, W. Ubachs: Appl. Opt. **40**, 4416 (2001)
44 I. Labazan, S. Rudic, S. Milosevic: Chem. Phys. Lett. **320**, 613 (2000)
45 R.T. Jongma, M.G.H. Boogarts, I. Holleman, G. Meijer: Rev. Sci. Instrum. **66**, 2821 (1995)
46 J.T. Hodges, J.P. Looney, R.D. v. Zee: Appl. Opt. **35**, 4112 (1996)
47 R.D. v. Zee, J.T. Hodges, J.P. Looney: Appl. Opt. **18**, 3951 (1999)
48 R.L. Stolk, J.J. ter Meulen: Diamond Relat. Mater. **8**, 1251 (1999)
49 X. Mercier, L. Pillier, A. Bakali, M. Carlier, J.F. Pauwels, P. Desgroux: Faraday Discuss. **119**, 305 (2001)
50 L. Pillier, C. Moreau, X. Mercier, J.F. Pauwels, P. Desgroux: Appl. Phys. B **74**, 427 (2002)
51 X. Ouyang, P.L. Varghese: Appl. Opt. **29**, 4884 (2003)